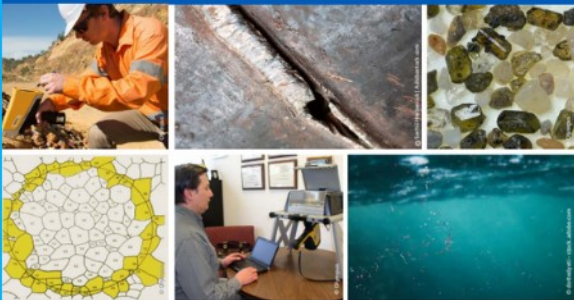




2nd Advanced Optical Metrology Compendium

Advanced Optical Metrology

Geoscience | Corrosion | Particles | Additive Manufacturing: Metallurgy, Cut Analysis & Porosity



EVIDENT
OLYMPUS

WILEY

The latest eBook from **Advanced Optical Metrology**.
Download for free.

This compendium includes a collection of optical metrology papers, a repository of teaching materials, and instructions on how to publish scientific achievements.

With the aim of improving communication between fundamental research and industrial applications in the field of optical metrology we have collected and organized existing information and made it more accessible and useful for researchers and practitioners.

EVIDENT
OLYMPUS

WILEY

Bioactive Nanogels Mimicking the Antithrombogenic Nitric Oxide-Release Function of the Endothelium

Aisa Hosseinejad, Nadine Ludwig, Sina Mersmann, Patrick Winnerbach, Christian Bleilevens, Rolf Rossaint, Jan Rossaint, and Smriti Singh*

Nitric oxide (NO) plays a significant role in controlling the physiology and pathophysiology of the body, including the endothelial antiplatelet function and therefore, antithrombogenic property of the blood vessels. This property of NO can be exploited to prevent thrombus formation on artificial surfaces like extracorporeal membrane oxygenators, which when come into contact with blood lead to protein adsorption and thereby platelet activation causing thrombus formation. However, NO is extremely reactive and has a very short biological half-life in blood, so only endogenous generation of NO from the blood contacting material can result into a stable and kinetically controllable local delivery of NO. In this regards, highly hydrophilic bioactive nanogels are presented which can endogenously generate NO in blood plasma from endogenous NO-donors thereby maintaining a physiological NO flux. It is shown that NO releasing nanogels could initiate cGMP-dependent protein kinase signaling followed by phosphorylation of vasodilator-stimulated phosphoprotein in platelets. This prevents platelet activation and aggregation even in presence of highly potent platelet activators like thrombin, adenosine 5'-diphosphate, and U46619 (thromboxane A₂ mimetic).

1. Introduction

Morbidity arising from material-induced thrombosis and infection is the major challenge when foreign materials get in contact to blood such as vascular grafts, intravascular catheters or in oxygenators present in extracorporeal membrane oxygenation (ECMO) systems or heart lung machines.^[1,2] ECMO is a life saving measure for patients suffering from acute respiratory distress syndrome (ARDS), chronic obstructive pulmonary lung disease, cystic fibrosis, or other respiratory diseases with fulminant affection of the lungs, if the maximum ventilation therapy fails to achieve sufficient oxygenation.^[3,4] ARDS triggered by the recent COVID19 pandemic, led to several ECMO applications around the world. Efficient functioning of the ECMO- and other similar systems depends on the blood-contacting biomaterials used in the device


to oxygenate the blood.^[5] In contrast to the healthy luminal endothelium with an inherent active thrombosis-^[6,7] and pathogenesis-resistance,^[8] artificial surfaces promote adverse interactions with blood components to stimulate thrombus formation and inflammation through a complex series of interconnected processes that set in by protein adsorption.^[9–12] Rapid protein adsorption subsequently leads to the structural and functional changes of proteins owing to the changes in the conformation and interaction at the surface interface. This is modulated by series of enthalpic and entropic changes in the formed surface-water-protein system.^[11,13,14] Once adsorbed, the proteins are recognized by glycoprotein receptors (GPIIb/IIIa) on the platelet surface^[11,15] causing platelet adhesion and aggregation.^[16] Upon platelet stimulation, the transduction of inside-out signals initiates the conformational change of GPIIb/IIIa.^[17–19] This conformational change increases the binding affinity of the receptor to the immobilized fibrinogen and/or other adsorbed protein ligands on the surface leading to the platelet activation.^[9,20,21] Activated platelets trigger the secretion of dense granular agonists such as platelets factor 4, adenosine 5'-diphosphate (ADP), thromboxane A₂ (TxA₂), and serotonin^[22–25] in an autocrine or paracrine manner^[26] to recruit more platelets for further adhesion, activation and aggregation on a surface.^[11] Platelet stimulation also causes translocation of P-selectin proteins (CD62P) from the platelets' alpha granules

A. Hosseinejad, S. Singh
DWI—Leibniz-Institute for Interactive Materials e.V. Forckenbeckstr. 50
52056 Aachen, Germany
E-mail: singh@dw.rwth-aachen.de

N. Ludwig, S. Mersmann, J. Rossaint
Department of Anesthesiology
Intensive Care and Pain Medicine
University Hospital Münster
Albert-Schweitzer-Campus 1, Bldg. A1, 48149 Münster, Germany

P. Winnerbach, C. Bleilevens, R. Rossaint
Department of Anesthesiology
University Hospital RWTH Aachen
Pauwelsstraße 30, 52074 Aachen, Germany

S. Singh
Max-Planck-Institut für medizinische Forschung
Jahnstraße 29, 69120 Heidelberg, Germany

 The ORCID identification number(s) for the author(s) of this article can be found under <https://doi.org/10.1002/sml.202205185>.

© 2023 The Authors. Small published by Wiley-VCH GmbH. This is an open access article under the terms of the Creative Commons Attribution-NonCommercial License, which permits use, distribution and reproduction in any medium, provided the original work is properly cited and is not used for commercial purposes.

DOI: 10.1002/sml.202205185

to their plasma membrane, which interacts with P-Selectin Glycoprotein Ligand-1 (PSGL-1) on neutrophils and endothelial cells and thereby amplifies the thrombogenicity and making the pathogenesis of the inflammatory response.^[27] The formed platelet aggregation concomitant with captured red blood cells and leukocytes is stabilized by crosslinked fibrin strands and results in a stable insoluble platelet-fibrin clot.^[28]

Hence improving the hemocompatibility of biomaterials can assure the efficiency and longevity of indwelling biomedical devices, as well as reduction of hemorrhagic risks and other hemostatic disorders arising from the use of excessive anticoagulants.^[29]

In general, platelet aggregation and coagulation do not occur in intact blood vessel. This is essentially due to the nitric oxide (NO)-dependent inhibition of platelet adhesion to the sub-endothelium, preventing platelet activation, aggregation, and ultimately thrombus formation. The main driving force here is NO-mediated activation of the soluble guanylate cyclase (sGC) in platelets leading to an increase of cyclic guanosine monophosphate (cGMP) concentration.^[30] Upon binding of NO to heme group of sGC,^[12,31] the conversion of guanosine triphosphate (GTP) to cGMP starts triggering a variety of further downstream effects including the activation of cGMP-dependent protein kinase (PKG) and the subsequent vasodilator-stimulated phosphoprotein (VASP) phosphorylation. Phosphorylated VASP reduces the activity of platelet $\alpha\text{IIb}\beta_3$ integrin (GPIIb/IIIa) and eventually leads to inhibition of platelet activation and aggregation.^[32–34] Endothelium-derived NO has an estimated flux of $(0.5\text{--}4) \times 10^{-10} \text{ mol cm}^{-2} \text{ min}^{-1}$ in blood, which means amount of NO released in a particular area in a defined time frame.^[35] However, the released NO is rapidly scavenged by oxygenated hemoglobin and myoglobin to produce nitrate. In the context of exploiting antithrombogenic potential of NO its short biological half-life limits its efficacy in reaching the target site. To harness the desired therapeutic outcome of NO for applying in biomaterials, it should be sustainably released in the right dose at the right place. In this regard, polymeric nanomaterials offer versatile possibilities to overcome this challenge.

To achieve this we prepared and systematically characterized a NO generating platform based on highly hydrophilic nanogels (NGs) with diselenide crosslinks. The diselenide bonds catalyze and sustain the endogenous generation of NO from an endogenous pool of physiological NO-donors. From the standpoint of practical applications, nanoparticles hold a great promise owing to their high surface area, uniform dispersion, and stability. We further investigated the pathway of released NO mediated by the synthesized nanogels from NO-reservoirs in order to understand how closely the proposed nanogels are able to mimic the physiological mechanism of NO-release regarding the platelet inhibition. The effect of NO-release from the prepared nanogels (NOrel-NGs) on human platelets was evaluated by assessing the level of GPIIb/IIIa activation and mobilization of P-selectin via flow cytometry. Additionally, the changes in platelet signaling upon NO-release were examined by analyzing VASP phosphorylation using western blot assays. We observed that NOrel-NGs showed a strong inhibitory effect on platelet activation even in presence of potent platelet activators like thrombin, ADP and U46619 (9,11-dioxy-11 α ,9 α -methanoepoxyprostaglandin F2 α ; thromboxane A2 mimetic) evidently corroborating the sufficient generation of phosphorylated

VASP via the activation of the physiologically known cGMP-PKG signaling pathway of platelet modulation.

2. Results and Discussion

2.1. Preparation and Characterization of Diselenide Incorporated p(HPMA-co-CBMAA) Nanogels

For the synthesis of the nanogels two highly hydrophilic non-fouling monomers *N*-(2-hydroxypropyl)methacrylamide (HPMA) and zwitterionic carboxybetaine methacrylamide (CBMAA) in a molar ratio of 17:3 were used. HPMA was synthesized by Schotten-Baumann condensation of methacryloyl chloride and 1-aminopropan-2-ol as described in the literatures.^[36,37] The successful synthesis of HPMA was demonstrated by ¹H-NMR indicating the characteristic signals (Figure S1, Supporting Information). Zwitterionic CBMAA was synthesized by opening of oxetane ring on β -propiolactone in reaction with *N*-[3-(dimethylamino)propyl]methacrylamide.^[38,39] Figure S2 in the Supporting Information shows the characteristic signals of successfully synthesized CBMAA. The p(HPMA-co-CBMAA) based nanogels were crosslinked by incorporation of diselenide bearing crosslinker DSeBAP, which was synthesized by the reaction of allyl glycidyl ether (AGE) with bis(trimethylsilyl)selenide (BTMSS) in presence of tetrabutylammonium fluoride hydrate (TBAF). The regioselective attacking of the seleno nucleophile on the less hindered side of the oxirane followed by the oxidation of the formed selenosilane (selenol) intermediate leads to the formation of diselenide crosslinker (Scheme S1, Supporting Information).^[40]

The structure of crosslinker (Figure S3A, Supporting Information) was characterized using ¹H- (Figure S3B, Supporting Information) and ⁷⁷Se-NMR (Figure S3C, Supporting Information). As depicted in Figure S3B in the Supporting Information, the multiplet peaks at 3.10 ppm assign to the methylene protons of Se-CH₂ indicating the formation of seleno organic bond on the primary structure of AGE. The characteristic double bond peaks of allyl substituents are observable at 5.25 and 5.90 ppm. The formation of diselenide bond was monitored by using ⁷⁷Se-NMR spectrum (Figure S3C, Supporting Information). The sharp singlet peaks at 290 and 291 ppm are attributed to the diselenide bonds formed in a diastereoisomeric mixture of crosslinker. The Raman spectroscopy was of use to further structural evaluation of diselenide crosslinker (Figure S3D, Supporting Information). The bands appearing at 2926 and 1646 cm⁻¹, respectively belong to the stretching vibration of methylene groups and allylic double bond in accordance with the structure of AGE as a base reagent. Compared to the lower frequency region (below 500 cm⁻¹) of AGE spectrum, the Raman spectrum of crosslinker obviously demonstrates the characteristic stretching mode of Se-Se at 290 cm⁻¹, which confirms the formation of diselenide bond.

Diselenide incorporated p(HPMA-co-CBMAA) nanogels (DiSe NGs) were prepared by free radical emulsion polymerization using a nonaqueous (oil in oil) miniemulsion, which is composed of two immiscible nonaqueous organic solvents including the combination of alcohols.^[41,42] Herein, the miniemulsion was prepared by ultrasonically dispersing a 1:10 volume of methanol in nonpolar hexadecane.

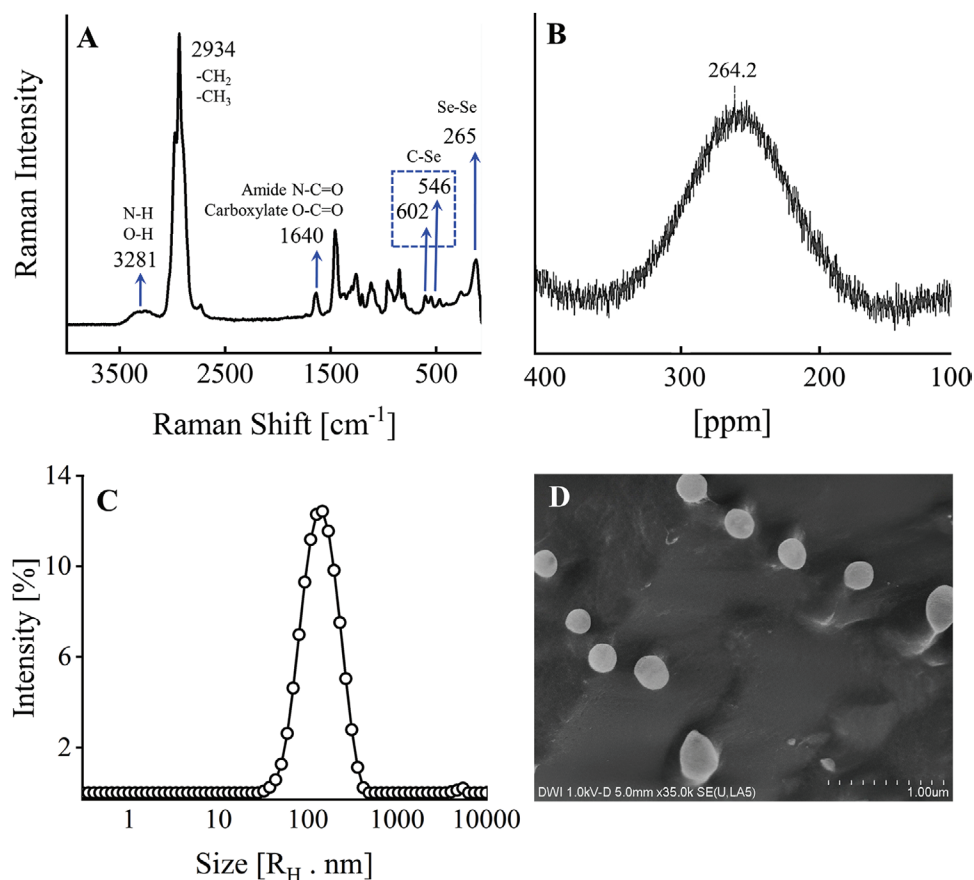


Figure 1. A) Raman spectrum of the DiSe NG revealing the presence of selenium in the lower-frequency region. B) Solid state ^{77}Se -NMR (600 MHz, D_2O) of the nanogel showing the characteristic diselenide peak. C) DLS analysis of the particle size distribution. D) Cryo-FESEM imaging of NOrel-NGs bearing a zeta potential of -6.15 ± 1.08 mV.

Since the DSeBAP crosslinker is nonsoluble in water, methanol was used as a dispersed phase (monomeric phase), since the both hydrophilic monomers and the initiator were also well methanol-soluble. It is known that allyl compounds including allyl ether derivations like the prepared DSeBAP crosslinker have a low polymerization rate arising from a degradative chain transfer to the monomer.^[43–45] Due to the temperature limit owing to the application of methanol as a solvent, the reaction rate of the crosslinker was improved by addition of phosphoric acid to the dispersed/monomeric phase in a molar ratio of 10:1 based on the moles of crosslinker. The increased acidity of the media stabilizes the proton on the carbon located at α -position and mutually increases the basicity of the monomer followed by reduction of the degradative chain transfer being converted into an effective one.^[46] The other parameters to achieve a stable colloidal system (Table S1, Supporting Information) were optimized according to our previous work. After ultrasonication, the polymerization initiated within the stabilized dispersed methanol droplets.^[47]

The Raman spectrum shows the structural characteristics of the nanogels (Figure 1A). The peak appearing at 1640 cm^{-1} is attributed to the typical $\text{C}=\text{O}$ band of the amide and carboxylate groups in HPMA and CBMAA. Moreover, the Raman reveals the incorporation of diselenide within the nanogel-network by demonstrating a dominant peak at 265 cm^{-1} assigning the stretching mode of Se-Se. The incorporation of diselenide

in the polymeric system of HPMA-co-CBMAA is additionally confirmed by solid state ^{77}Se -NMR indicating a broad peak at 264.2 ppm (Figure 1B). The wide width of signal in the solid state NMR is arising from the effect of strong chemical shift anisotropy, orientation-dependent interactions and dipolar-dipolar coupling.^[48] The dynamic light scattering (DLS) analysis (Figure 1C) and the cryo-Field emission scanning electron microscopy (FESEM) imaging (Figure 1D) of DiSe NGs suggest the well-defined spherical morphology and the monodispersity of synthesized nanogels with an average hydrodynamic radius (R_H) of 150 nm (polydispersity index (PDI) 0.17) in the swollen state. The nanogels were also characterized for zeta potential in phosphate-buffered saline (PBS, pH 7.4) at $25\text{ }^\circ\text{C}$ and the results demonstrated an average zeta potential of -6.15 ± 1.08 mV ($n = 5$) as anticipated for the zwitterionic nanogels.

The proton NMR of nanogels reveals the molar ratio of HPMA to CBMAA (Figure S4, Supporting Information). Compared to the reference *N,N'*-methylenebis(acrylamide) (MBAA) crosslinked nanogels (MBAA NGs) synthesized with the same molar composition of the reactants, the characteristic peaks of HPMA [1H , $\text{C}(\text{OH})-\text{H}$] and CBMAA [2H , $-\text{CH}_2-(\text{CO})-\text{O}-$] are observable at 3.90 and 2.60 ppm, respectively. The integral ratio of the featured peaks is attributed to the molar ratio of corresponded hydrogens, which further exhibits the molar ratio of the copolymerized HPMA to CBMAA ($17 \times 1\text{H}$):($3 \times 2\text{H}$) in

agreement with the feed composition. This set molar ratio provides a significant antifouling property as previously shown in our latest work.^[49] The well-known antifouling properties of HPMA as a simple hydroxyl-containing polymer owing to its strong ion hydration shell (ionic solvation) is well established.^[50,51] The strong electrostatically induced surface hydration (ionic solvation) along with the electroneutrality and hydrogen-bonding interactions of zwitterionic polymers gives rise to the high wettability and significantly minimized nonspecific protein adsorption (ultralow fouling) in the complex biological media.^[39,52–54]

2.2. NO-Generation

To investigate the bioinspired catalytic function of the nanogels to release NO, physiologically available NO donor S-nitrosoglutathione (RSNO) was used. Mechanistically, the interaction of DiSe NGs with RSNO results in generation of NO in presence of physiologically available tripeptide glutathione (GSH). GSH reduces the diselenides to provide the primary active species: selenol/selenolate (RSeH/RSe⁻) which decomposes NO-donors to release NO. Meanwhile, the selenenyl sulfide formed (RSe-SG) is again reduced by GSH to regenerate (RSeH/RSe⁻) and thus the catalytic reaction continues.

The effect of NO-generation mediated by these nanogels was evaluated using a modified Griess test, which is a sensitive spectrophotometric method for the detection of nitrite (Figure S5A, Supporting Information). Since the direct measurement of NO is difficult, stable metabolites such as nitrites formed by the spontaneous oxidation of NO were used as its surrogates. In Griess test the diazotization of Griess reagent plays a principal role. The reaction of sulfanilic acid (the first Griess reagent) with nitrite quantitatively produces a diazonium salt. This salt can be coupled to *N*-(1-naphthyl)ethylenediamine (the second Griess reagent) and form an azo dye, which has a detectable absorbance at 548 nm. Remarkably, the direct conversion of the *N*-nitroso compound to NO by GSH is also feasible.^[55] However, the formation of diselenide is four order of magnitude higher than the disulfide species in an exchange reaction between selenium and

sulfur. Thereby, the NO-generation is rather catalyzed by selenolates than thiol molecules. Furthermore, the reaction of GSH with the diselenide is around three times faster compared to the reaction with S-nitroso compound ($k = (3.6 \pm 0.1) \times 10^5$ compared to $k = (1.3 \pm 0.2) \times 10^5$).^[56] Though the reaction of GSH with S-nitroso compound is, non-negligible, blank correction was made with GSH and RSNO without the NGs.

The NO-generating effect of NGs was evaluated using a variable concentration of NGs from 100 to 1000 $\mu\text{g mL}^{-1}$, which correspondingly increased the selenium content, while the concentration of RSNO (3 mg mL^{-1}) and GSH (2 mg mL^{-1}) were kept constant. The results showed an increase in the NO-release profile in a dose-dependent manner (Figure S5B, Supporting Information) confirming the postulated mechanism for the proposed system.

2.3. Endogenous Release of NO Prevents Platelet Activation

The effect of endogenous NO-generation mediated by NOrel-NGs in presence of S-nitrosoproteins was investigated on human platelets. Different concentration of NGs from 100 to 1000 $\mu\text{g mL}^{-1}$ were incubated in 1 mL of the fresh platelet rich plasma (PRP) of a healthy donor with concomitant addition of GSH (2 $\mu\text{g mL}^{-1}$) and RSNO (3 $\mu\text{g mL}^{-1}$) at room temperature. Using PRP provides a straightforward method to exclusively investigate the mechanism of biomimetic action of NOrel-NGs on pool of platelets. The used concentration of GSH and RSNO were in the range of their physiologically available concentration in blood. The effect of NO-release on the prevention of platelet activation was measured in different incubation times up to 240 min by flow cytometry (Figure 2A). This method applies for measuring the platelet activation by quantifying the expression of platelet p-selectin surface markers using fluorescent antibodies for CD61 (a marker of all platelets) and CD62P (expressed on activated platelets), respectively called CD61+ and CD62P+.^[57] Thereby, the ratio of CD62P+/CD61+ shows the percentage of the activated platelets in each sample, whereas the lower CD62P+/CD61+ is, the more is the inhibitory effect

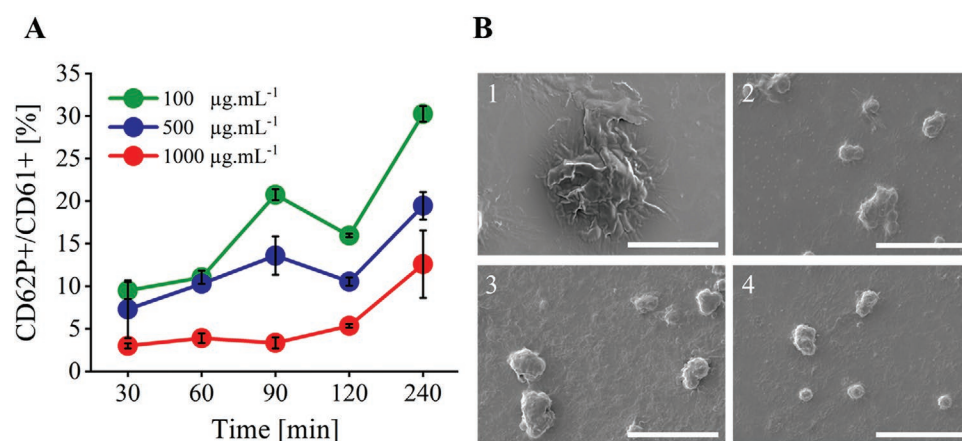


Figure 2. A) The ratio of activated platelets to the unstimulated ones exposed to the different concentrations of NO-generating nanogels at different time intervals. FACS was used to calculate the ratio of expressed CD62P+ to CD61+ on platelets. $n = 2$, CD62P+/CD61+ are presented as mean \pm SD. B) SEM images of the platelets morphology at room temperature after 240 min exposure to the different concentrations of NO-generating nanogels: 1) blank, 2) 100 $\mu\text{g mL}^{-1}$, 3) 500 $\mu\text{g mL}^{-1}$, and 4) 1000 $\mu\text{g mL}^{-1}$ (Scale bar: 20 μm).

on platelets induced by the generated NO from the NGs. Remarkably, in the absence of NGs platelets were highly aggregated and it was not possible to measure by fluorescence-activated cell sorting (FACS). The inhibitory effect of generated NO on the platelets was further verified by scanning electron microscopy (SEM) imaging after 240 min at room temperature (Figure 2B1–4). The SEM images clearly demonstrate that on increasing the concentration of NOrel-NGs, platelets activation is gradually prevented and consequently their aggregation is inhibited.

2.4. NOrel-NGs Inhibit the Activation of GPIIb/IIIa and Mobilization of CD62P in Human Platelets

To investigate the biological effect of NOrel-NGs, isolated washed human platelets were coincubated with supplemented NGs and a putative platelet stimulant (thrombin, ADP, collagen or U46619). Since NGs mitigate platelet activation most efficiently at a concentration of $1000 \mu\text{g mL}^{-1}$, all further experiments were performed according to our previous findings. The platelets were subsequently analyzed via flow cytometry concerning GPIIb/IIIa activation and CD62P mobilization (Figure 3). The NGs alone did not activate platelets, since coincubation without an additional stimulus did not cause a rise in activated GPIIb/IIIa or CD62P presence on the platelet surface. However, the stimulating effects of thrombin, ADP and U46619 on platelets were strongly inhibited by the addition of NGs, concerning both GPIIb/IIIa activation (Figure 3A) and CD62P mobilization (Figure 3B). Treatment with collagen did not affect the investigated parameters, which was also not altered by addition of NGs.

Measuring the high-affinity conformation of surface GPIIb/IIIa and mobilization of CD62P from alpha granules are commonly used markers to assess platelet activation via flow cytometry.^[58] GPIIb/IIIa is the most abundantly expressed receptor on the surface of platelets. Upon platelet stimulation, GPIIb/IIIa changes from a low-affinity into a high-affinity conformation and thus allows ligand binding of fibrinogen, fibronectin, and von Willebrand factor.^[59] On the contrary, P-selectin is a transmembrane protein that resides in the membrane of platelet alpha granules. Platelet stimulation causes translocation of P-selectin to the plasma membrane where it may interact with other cell receptors, like PSGL-1 on neutrophils and endothelial cells.^[27] Platelet stimulants such as thrombin, ADP, collagen and the thromboxan A_2 (TXA_2) analogon U46619 are potential candidates to affect GPIIb/IIIa activation and CD62P release.^[60] The serine protease thrombin is a pivotal activator of platelets executing its effector functions on human platelets mainly via the protease-activated receptors PAR1 and PAR4. Stimulation with thrombin results in activation of phospholipase C and an increase of intracellular Ca^{2+} levels, thereby promoting the release of pharmacologically active substances from granules.^[61] ADP and TXA_2 serve as secondary mediators in platelet activation, signal through standard receptor/ligand interactions and stimulate the heterotrimeric G protein coupled receptors $\text{P2Y}_1/\text{P2Y}_{12}$ and $\text{TP}\alpha/\text{TP}\beta$, respectively. Furthermore, collagen binding to its receptor GPIV is mediated by $\text{GPIIb}\alpha\text{-vWF}$ interactions on the extracellular matrix and triggers integrin

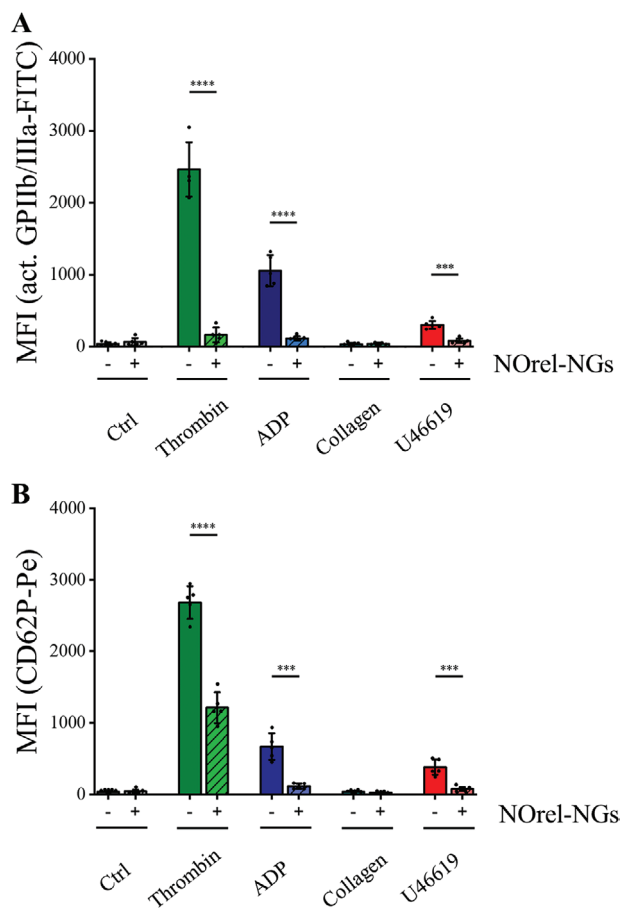


Figure 3. Activation of GPIIb/IIIa and mobilization of CD62P is significantly decreased by addition of supplemented NOrel-NGs. Human platelets were stimulated with thrombin (0.05 U mL^{-1}), ADP ($20 \mu\text{M}$), collagen ($25 \mu\text{g mL}^{-1}$) and U46619 ($5 \mu\text{M}$) for 10 min and supplemented with NOrel-NGs. Platelets were analyzed for A) GPIIb/IIIa activation and B) CD62P mobilization. $n = 5$, MFIs are presented as mean \pm SD, * $p < 0.05$, ** $p < 0.01$, *** $p < 0.001$, **** $p < 0.0001$

activation and granule release.^[26] The results highlight a strong inhibitory effect of the NGs on human platelets.

Since the combination of the supplements (GSH and RSNO) alone might already have an effect on platelet activation, platelets were stimulated also with thrombin and GSH/RSNO without further addition of NGs. GSH/RSNO clearly diminished platelet activation, but the effect of NO release by NGs outperforms the effect of GSH/RSNO on platelet activation (Figure 4). This underlines the enormous potential of using such NOrel-NGs as an antiplatelet coating material for medical devices coming into contact with blood.

2.5. NOrel-NGs Stimulate cGMP-PKG Signaling in Platelets

To analyze if the effect of the NOrel-NGs on platelets equal in vivo conditions, isolated washed human platelets were stimulated with thrombin and supplemented with NOrel-NGs. To trigger the catalytic function of the NGs, they were always used with GSH and RSNO supplementation. Phosphorylation

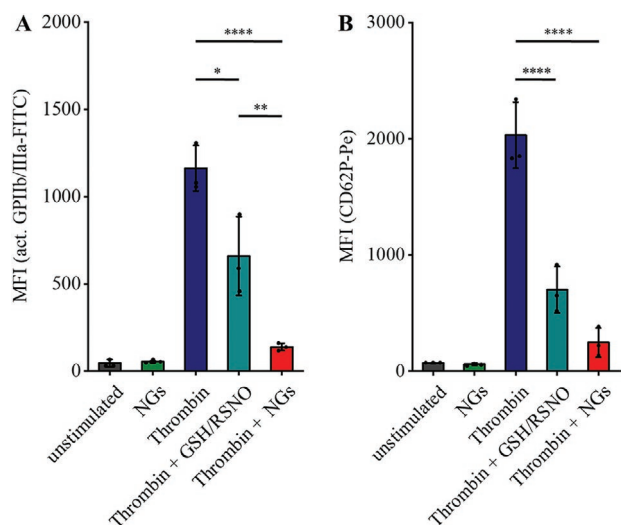


Figure 4. NGs potentiate the inhibitory effect of NO. Human platelets were stimulated with thrombin (0.05 U mL^{-1}) in presence of the supplemented NOrel-NGs (NGs) or reaction starter GSH and RSNO only (GSH/RSNO). Platelets were analyzed for A) GPIIb/IIIa activation and B) CD62P mobilization. $n = 3$, MFIs are presented as mean \pm SD, * $p < 0.05$, ** $p < 0.01$, *** $p < 0.001$, **** $p < 0.0001$.

of VASP, and thereby cGMP-PKG signaling, was assessed via western blot analysis. Endogenous NO initiates the activation of soluble guanylyl cyclase (sGC) in platelets.^[30] Upon binding of NO to heme group of sGC^[12,31] the conversion of GTP to cGMP is triggered,^[32–34] which is a significant secondary messenger molecule whose elevated intracellular level induces the variety of further downstream effects^[62] such as the activation of cGMP-PKG.^[63] This mediates the phosphorylation of Ser239 site of VASP. Ser239 phosphorylated VASP (pVASP) reduces the activity of platelet surface receptor $\alpha\text{IIb}\beta_3$ integrin and eventually leads to inhibition of platelets activation and

aggregation.^[64–66] The addition of NOrel-NGs supplemented with GSH and RSNO clearly result in phosphorylation of VASP. This is not only observed in presence of a platelet stimulant, but also in resting platelets. These results indicate that NO-release by NGs keep platelets in an inhibited state via cGMP-PKG signaling. Furthermore, the observed effect is not only based on the NO donor RSNO but is significantly increased by the NGs' presence (Figure 5). The findings support the antithrombogenic function of the NGs.

3. Conclusion

To attain an endogenous NO-delivery with a sustainable and controlled release rate of NO, highly hydrophilic NOrel-NGs were synthesized. The NGs incorporated diselenide crosslinks which acted as a catalytic center for continuous generation of NO from its endogenous source thereby, mimicking the function of native blood vessels lined by endothelium. In the presence of NOrel-NGs, the rate of platelet activation was drastically reduced. This effect was dependent on the concentration of the NGs and in turn the number of diselenide bridges in the NGs. The inhibitory effect of the NGs on platelets activation and aggregation was evaluated by expression of GPIIb/IIIa membrane receptor and P-selectin surface membrane protein of platelets, upon stimulation by potent platelet activators like thrombin, ADP, and thromboxane A2. The significant reduction in GPIIb/IIIa activation and CD62P mobilization supported the antithrombogenic effect of the NOrel-NGs. This effect was mainly due to the phosphorylation of VASP. A remarkable increase of pVASP in stimulated platelets in presence of NOrel-NGs corroborated the activation of cGMP-PKG signaling preventing platelet activation, analogous to in vivo conditions. These insightful results on the mechanism of action of the introduced NOrel-NGs reveal their promised potential for applying as an antiplatelet coating material on

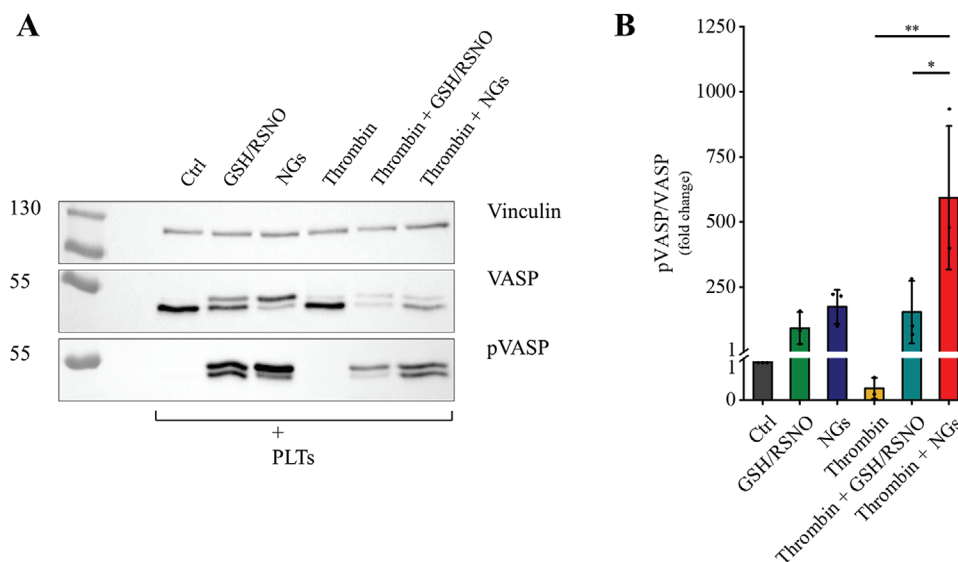


Figure 5. Nanogels increase VASP phosphorylation. Human platelets were stimulated with thrombin for 10 min in presence of the supplemented NOrel-NGs (NGs) or reaction starter GSH and RSNO only (GSH/RSNO). A) Western blots were plotted by B) densitometric analysis. $n = 3$, data are presented as mean \pm SD, * $p < 0.05$, ** $p < 0.01$.

blood-contacting biomedical surfaces including stents and catheters in our future in vivo studies. The local concentration of NO and the sustainment of its endogenous flux in such a system is physiologically regulated at the interface of the blood-contacting foreign surface highly dependent on the bioavailability of the endogenous NO-donors.

4. Experimental Section

Materials: Anhydrous dichloromethane (DCM), Span 80 (sorbitan monooleate), Tween 80 (polyethylene glycol sorbitan monooleate), *n*-hexadecane 99%, TBAF hydrate (98%), anhydrous sodium sulfate, *N*-[3-(dimethylamino)propyl]methacrylamide, 3-hydroxypropionic acid lactone (β -Propiolactone 97%), anhydrous tetrahydrofuran (THF), 1-allyloxy-2,3-epoxypropane (allyl glycidyl ether $\geq 99\%$), diethyl ether (DEE), ethanol 99%, phosphoric acid 85%, and MBAA 99% were all purchased from Sigma-Aldrich. 2-Methylprop-2-enoyl chloride (methacryloyl chloride 97%) and 2,2'-azobis(2-methylpropionamide) dihydrochloride (AMPA 97%) were purchased from Acros organics. 1-aminopropan-2-ol 98%, PBS (1 \times pH 7.4), sodium carbonate, L-glutathione reduced (GSH $\geq 98\%$), and S-nitrosoglutathione (GSNO $\geq 97\%$) were purchased respectively from abcr GmbH, Merck, Lonza AG, ChemPur, Carl Roth GmbH, and ChemCruz SCBT, respectively. Griess reagent kit (G-7921) was obtained from Thermo Fisher Scientific, which contains 0.1 w/v% (1 $\mu\text{g mL}^{-1}$) of *N*-(1-naphthyl)ethylenediamine dihydrochloride, 1 w/v% (10 $\mu\text{g mL}^{-1}$) of sulfanilic acid in 5% phosphoric acid and 1.0 mM sodium nitrite standard solution. All chemicals and reagents were of analytical grade and used as received without further purification.

Synthesis of HPMA: 1-Aminopropan-2-ol (22 g, 289 mmol, 1.0 eq) and sodium carbonate (34 g, 318 mmol, 1.1 eq) were mixed and stirred in 85 mL anhydrous DCM using a 500 mL three-neck flask immersed in an ice bath. 27 mL methacryloyl chloride (275 mmol, 0.95 eq) dissolved in 15 mL anhydrous DCM was added dropwise into the mixture for 2 h. Then the ice bath was removed and the reaction was proceeded for further 4 h at room temperature. The whole procedure was under N_2 gas. Anhydrous sodium sulfate (10 g) was added into the reaction mixture and filtered. The filtrate was concentrated under reduced pressure at 40 $^\circ\text{C}$ and further kept at -20 $^\circ\text{C}$ for overnight. The obtained crystals were filtered and recrystallized in acetone at -20 $^\circ\text{C}$. The purified solid was dried under reduced pressure after filtration and kept in a freezer (Yield 6 g, 10%).

Values of $^1\text{H-NMR}$ (300 MHz, D_2O , δ): 1.10 ppm (dd, 3H, $\text{CH}(\text{OH})-\text{CH}_3$), 1.90 ppm (s, 3H, $\text{C}(\text{CH}_2)-\text{CH}_3$), 3.20 ppm (m, 2H, $\text{NH}-\text{CH}_2$), 3.90 ppm (m, 1H, $\text{C}(\text{OH})-\text{H}$), 5.40 ppm (m, 1H, $\text{C}-\text{CH}_2$), 5.60 ppm (m, 1H, $\text{C}-\text{CH}_2$).

Synthesis of the Zwitterionic CBMAA: 36 mL (200 mmol, 1.45 eq.) *N*-[3-(dimethylamino)propyl]methacrylamide and 9 mL (138 mmol, 1.0 eq.) β -propiolactone were respectively added in 200 and 80 mL anhydrous THF. The solution of *N*-[3-(dimethylamino)propyl]methacrylamide was cooled to -4 $^\circ\text{C}$ using a cooling bath with sodium chloride. β -propiolactone was dropwise fed into *N*-[3-(dimethylamino)propyl]methacrylamide for 15 min. The whole procedure was performed under N_2 gas. The solution was stirred for further 15 min at 4 $^\circ\text{C}$ and kept in a fridge (2–8 $^\circ\text{C}$) for 1–2 d. The white powder of the purified product was obtained by washing the solids with 20 mL anhydrous THF ($\times 3$) and 20 mL DEE ($\times 1$) and drying under reduced pressure (Yield 11 g, 34%).

Values of $^1\text{H-NMR}$ (300 MHz, D_2O , δ): 1.90 ppm (s, 3H, $\text{C}(\text{CH}_2)-\text{CH}_3$), 2.00 ppm (m, 2H, $\text{C}(\text{CH}_2)-\text{H}_2$), 2.60 ppm (t, 2H, $\text{C}(\text{CH}_2)-\text{H}_2$), 3.00 ppm (s, 6H, $\text{N}-\text{CH}_3$), 3.30 ppm (m, 4H, $\text{N}-(\text{CH}_2)-\text{CH}_2$), 3.50 ppm (t, 2H, $\text{N}-\text{CH}_2$), 5.40 ppm (m, 1H, $\text{C}-\text{CH}_2$), 5.70 ppm (m, 1H, $\text{C}-\text{CH}_2$).

Synthesis of 3,3'-Diselenediylbis[1-(allyloxy)propan-2-ol] (DSeBAP): 104 μL (0.9 mmol, 1.0 eq.) AGE, and 351 μL (1.4 mmol, 1.60 eq.) BTMSS were added in 3 mL anhydrous THF. The solution was dropwise treated with 561 μL (0.6 mmol, 0.64 eq.) TBAF and stirred at room temperature for further 4 h. The whole procedure was performed under N_2 gas. The mixture was diluted with 8 mL DEE and washed with 5 mL water using a separatory funnel. The solution was dried with anhydrous sodium

sulfate and the solvent (DEE) was removed under reduced pressure to obtain the crude yellowish product (Yield 120 mg, 57%).

Values of $^1\text{H-NMR}$ (300 MHz, CDCl_3 , δ): 3.10 ppm (m, 4H, $\text{Se}-\text{CH}_2$), 3.40 ppm (m, 4H, $\text{C}(\text{CH}_2)-\text{O}$), 4.00 ppm (m, 6H, $\text{O}-\text{CH}_2$ and $\text{C}(\text{OH})-\text{H}$), 5.20 ppm (d, 2H, $\text{CH}-\text{CH}_2$), 5.30 ppm (d, 2H, $\text{CH}-\text{CH}_2$), 5.90 ppm (m, 2H, $\text{C}(\text{CH}_2)-\text{H}$).

Synthesis of Diselenide-Containing DSeBAP Incorporated Nanogels: The diselenide incorporated nanogels were prepared via an inverse miniemulsion polymerization using 3,3'-diselenediylbis[1-(allyloxy)propan-2-ol] (DSeBAP) crosslinker. 10 mL of hexadecane as a continuous phase consisted of 280 mg of Span 80 and Tween 80 in a weight ratio of 3:1. HPMA (122 mg, 0.80 mmol, 17 eq.), CBMAA (36 mg, 0.14 mmol, 3 eq.), and DSeBAP (12 mg, 0.03 mmol) were dissolved in 0.5 mL of methanol (dispersed phase) and 17.5 μL of phosphoric acid 85% followed by addition to the organic phase. The mixture was vigorously stirred for 5 min at room temperature and subjected to ultrasonication in a rosette cooling cell immersed in water for 5 min. The sonication parameters were kept at 50% amplitude in a set pulse regime (0.9 s sonication, 0.1 s pause) using a Branson 250 W sonifier and a micro tip of 6.4 mm in diameter. The thermosensitive cationic initiator AMPA (8.4 mg, 0.03 mmol) dissolved in 0.5 mL PBS was added dropwise to the mixture along the ultrasonication treatment for further 5 min. The mixture was sonicated for another 5 min and then purged with N_2 gas. The emulsion was heated to 60 $^\circ\text{C}$ to initiate the polymerization by AMPA while it was stirred at 700 rpm under an inert atmosphere for 24 h. The organic phase was removed by centrifuging the emulsion at 10 000 rpm for 5 min. The nanogels were carefully washed with hexadecane (3 \times 10 mL) and dialyzed against distilled water for 7 d. The obtained nanogels were freeze dried and kept in 2–8 $^\circ\text{C}$.

Modified Griess Test: Equal volumes of *N*-(1-naphthyl)ethylenediamine dihydrochloride and sulfanilic acid were mixed to form the sufficient Griess reagent for an immediate experiment. 130 μL of nanogel aqueous dispersion in desired concentrations (100, 500, and 1000 $\mu\text{g mL}^{-1}$) was mixed with 10 μL of each GSH (2 mg mL^{-1}) and GSNO (3 mg mL^{-1}) (volume ratio 13:1:1). Then 20 μL of Griess reagent and 130 μL of deionized water were added to the mixture followed by the incubation for 30 min at room temperature. A photometric reference blank was prepared prior measuring containing 10 μL of GSH (2 mg mL^{-1}), 10 μL of GSNO (3 mg mL^{-1}), 20 μL of Griess reagent, and 280 μL of deionized water. The absorbance of the samples was measured in a spectrophotometric microplate reader at the optimum wavelength of 548 nm. The nitrite concentration corresponding to the absorbance was calculated from the NO_2^- standard plot after subtraction of the background absorbance.

Platelets Activation: The antithrombotic effect of DiSe NGs was evaluated by studying the activation and aggregation of human platelets. Fresh human platelet-rich plasma (PRP) with the concentration of 4×10^7 plt mL^{-1} was obtained from whole blood of a healthy donor by centrifuging at 68 \times g for 7 min. 867 μL aqueous dispersion of nanogels in desired concentrations (100, 500, and 1000 $\mu\text{g mL}^{-1}$) was added to 1 mL of prepared PRP in a 2 mL safe-lock tube followed by addition of 66.5 μL from each GSH (2 $\mu\text{g mL}^{-1}$) and GSNO (3 $\mu\text{g mL}^{-1}$) (volume ratio 13:1:1). The samples were mixed using a rotating mixer at 37 $^\circ\text{C}$. The platelet activation was monitored in different time points of 30, 60, 120, and 240 min using FACS flow cytometry method. For this measurement the platelet samples were diluted (1:50) in tyrodes buffer and incubated with fluorescein isothiocyanate-conjugated and phycoerythrin-conjugated CD61 and CD62P or their appropriate isotype controls for 15 min at room temperature. After staining, platelets were fixed for analysis by FACS Canto Flow Cytometer (BD Biosciences, San Jose, CA, USA).

The morphology of platelets was further studied by SEM imaging with an acceleration voltage between 1 and 20 kV. For the analysis, the samples were fixed with 4% paraformaldehyde (PFA) solution in PBS for 15 min followed by a dehydration step using 0, 30, 50, 70, and 100% mixtures of PBS: ethanol and drying with hexamethyldisilazane. After the fixation, the samples were sputter-coated by a 10 nm layer of gold/palladium (80:20) using an ACE 600 sputter coater (Leica, Germany).

Flow Cytometry Analysis: Human blood was obtained from healthy adult individuals. Anticoagulated (3.2% sodium citrate, Sarstedt) whole blood was centrifuged at $68 \times g$ for 7 min to generate PRP with the concentration of 4×10^7 plt mL⁻¹. Platelets were pelleted by centrifuging PRP for $790 \times g$ for 5 min. All centrifugation steps were performed in soft mode to minimize platelet pre-stimulation. Pelleted platelets were resuspended in modified Tyrode's buffer (20 mM N-2-hydroxyethylpiperazine-N'-2ethane sulphonic acid (HEPES), 136 mM NaCl, 2.6 mM KCl, 12 mM NaHCO₃, 5.5 mM D-glucose, 2 mM CaCl₂, and 1 mM MgCl₂) and the cell count was adjusted to 40×10^6 platelets mL⁻¹. Platelets were supplemented with 1 mg mL⁻¹ NO-releasing nanogels, 0.3 mM RSNO and 0.2 mM GSH and 2.5×10^6 cells were stimulated with Thrombin (0.05 U mL⁻¹, Sigma), ADP (20 μM, Sigma), Collagen (25 μg mL⁻¹, Chrono-Log) or U46619 (5 μM, Tocris) for 10 min. Antibodies detecting CD41 (HIP8, BioLegend), CD62P (AK-4, BioLegend), and activated GPIIb/IIIa (Pac-1, BD Biosciences) were added simultaneously. Samples were fixed with 1% PFA for 15 min and analyzed in an FACS Canto II flow cytometer (BD Biosciences). Mean fluorescence intensities were determined using FlowJo software (version 7.6) by gating on CD41 positive platelets.

Western Blot: Stimulated platelets (2.5×10^6) were lysed with Triton-based lysis buffer (50 mM Tris, 150 mM NaCl, 0.5% Triton, 0.5 mM ethylenediaminetetraacetic acid (EDTA) in ddH₂O, supplemented with phosphatase and protease inhibitors (both from Roche)) on ice for 30 min. Lysates were boiled with 3× Laemmli sample buffer, run on 10% sodium dodecyl sulphate-polyacrylamide gel electrophoresis (SDS-PAGE) gels and immunoblotted using antibodies against pVASP (Cell Signaling, 1:1000), VASP (Cell Signaling, 1:500) and Vinculin (Cell signaling, 1:1000). Densitometric analyses were performed with Image Lab software (BioRad).

Statistics: Statistical analysis was performed with GraphPad Prism (version 9.3.0). Data distribution was assessed using Shapiro-Wilk or Kolmogorov-Smirnov test. Significance of two groups was tested with an unpaired Wilcoxon-test or t-test, while more than two groups were compared using Kruskal-Wallis test or an ordinary one-way analysis of variance (one-way ANOVA). Data are presented as means ± standard deviation SD and *n* describes the number of independent experiments.

Ethical Statement: All experiments were performed in accordance with the Helsinki declaration and were approved by the ethics committee at committee at the University Hospital, RWTH Aachen (EK134/20) and Münster. Informed consents were obtained from human participants of this study.

Supporting Information

Supporting Information is available from the Wiley Online Library or from the author.

Acknowledgements

A.H. and N.L. contributed equally to this work. The authors acknowledge the financial support by the Deutsche Forschungsgemeinschaft (DFG, German Research Foundation) via Schwerpunktprogramm "Towards an Implantable Lung" grant numbers DFG RO 2000/23-1 to R.R., SI 2164/2-1 to S.S., and RO 4537/3-1 and RO 4537/4-1 to J.R.

Open access funding enabled and organized by Projekt DEAL.

Conflict of Interest

The authors declare no conflict of interest.

Data Availability Statement

The data that support the findings of this study are available in the Supporting Information of this article.

Keywords

antithrombogenic, cGMP-PKG signaling, nanogels, nitric oxide, platelets inhibition

Received: August 23, 2022

Revised: November 7, 2022

Published online:

- [1] S. Doymaz, *J. Intensive Crit. Care* **2018**, *04*, 12.
- [2] M. Weber, H. Steinle, S. Golombek, L. Hann, C. Shlensak, H. P. Wendel, M. Avci-Adali, *Front. Bioeng. Biotechnol.* **2018**, *6*, 99.
- [3] P. Gupta, R. McDonald, C. W. Chipman, M. Stroud, J. M. Gossett, M. Imamura, A. T. Bhutta, *Ann. Thoracic Surg.* **2012**, *93*, 1584.
- [4] H. Nolan, D. Wang, J. B. Zwischenberger, *Organogenesis* **2011**, *7*, 23.
- [5] D. F. Williams, *Biomaterials* **2009**, *30*, 5897.
- [6] G. T. Housholder, *J. Oral Maxillofac. Surg.* **1991**, *49*, 507.
- [7] J. W. Yau, H. Teoh, S. Verma, *BMC Cardiovasc. Disord.* **2015**, *15*, 130.
- [8] T. T. Keller, A. T. A. Mairuhu, M. D. de Kruijf, S. K. Klein, V. E. A. Gerdes, H. ten Cate, D. P. M. Brandjes, M. Levi, E. C. M. van Gorp, *Cardiovasc. Res.* **2003**, *60*, 40.
- [9] X. Liu, L. Yuan, D. Li, Z. Tang, Y. Wang, G. Chen, H. Chen, J. L. Brash, *J. Mater. Chem. B* **2014**, *2*, 5718.
- [10] M. Mulder, I. Fawzy, M. Lancé, *Neth. J. Crit. Care* **2018**, *26*, 6.
- [11] I. Jaffer, J. Fredeburgh, J. Hirsh, J. Weitz, *J. Thromb. Haemostasis* **2015**, *13*, S72.
- [12] Y. Wo, E. J. Brisbois, R. H. Bartlett, M. E. Meyerhoff, *Biomater. Sci.* **2016**, *4*, 1161.
- [13] H. T. Aiyelabegan, E. Sadroddiny, *Biomed. Pharmacother.* **2017**, *88*, 956.
- [14] M. Ozboyaci, D. Kokh, R. Wade, *Phys. Chem. Chem. Phys.* **2016**, *18*, 10191.
- [15] Z. M. Ruggeri, G. L. Mendolicchio, *Circ. Res.* **2007**, *100*, 1673.
- [16] B. Vadasz, P. Chen, I. Yougbaré, D. Zdravic, J. Li, C. Li, N. Carrim, H. Ni, *Genes Dis.* **2015**, *2*, 173.
- [17] A. Coutinho, C. García, J. González-Rodríguez, M. P. Lillo, *Biophys. Chem.* **2007**, *130*, 76.
- [18] P. J. Sims, M. Ginsberg, E. Plow, S. Shattil, *J. Biol. Chem.* **1991**, *266*, 7345.
- [19] J. Huang, X. Li, X. Shi, M. Zhu, J. Wang, S. Huang, X. Huang, H. Wang, L. Li, H. Deng, *J. Hematol. Oncol.* **2019**, *12*, 26.
- [20] M. Nieberler, U. Reuning, F. Reichart, J. Notni, H.-J. Wester, M. Schwaiger, M. Weinmüller, A. Räder, K. Steiger, H. Kessler, *Cancers* **2017**, *9*, 116.
- [21] A. Rana, E. Westein, B. e. Niego, C. E. Hagemeyer, *Front. Cardiovasc. Med.* **2019**, *6*.
- [22] S.-H. Yun, E.-H. Sim, R.-Y. Goh, J.-I. Park, J.-Y. Han, *Biomed Res. Int.* **2016**, *2016*, 9060143.
- [23] H. Hosseinzadegan, D. Tafti, *Thromb. Haemostasis Res.* **2017**, *1*, 1008.
- [24] A. D. Michelson, *Nat. Rev. Drug Discovery* **2010**, *9*, 154.
- [25] K. Ghoshal, M. Bhattacharyya, *Sci. World J.* **2014**, *2014*, 781857.
- [26] J. Rivera, M. L. Lozano, L. Navarro-Núñez, V. Vicente, *haematologica* **2009**, *94*, 700.
- [27] B. Furie, B. C. Furie, R. Flaumenhaft, *Thromb. Haemostasis* **2001**, *86*, 214.
- [28] J. W. Weisel, R. I. Litvinov, in *Fibrous Proteins: Structures and Mechanisms*, Springer, New York **2017**, *82*, 405.
- [29] H. J. Cho, D. W. Kim, G. S. Kim, I. S. Jeong, *Chonnam Med. J.* **2017**, *53*, 110.
- [30] G. Zhang, B. Xiang, A. Dong, R. C. Skoda, A. Daugherty, S. S. Smyth, X. Du, Z. Li, *Blood* **2011**, *118*, 3670.
- [31] A. Smolenski, *J. Thromb. Haemostasis* **2011**, *10*, 167.

- [32] A. Bradley Levine, A. B. Levine, D. Punihaole, T. B. Levine, *Cardiology* **2012**, 122, 55.
- [33] S. Lambden, *Intensive Care Med. Exp.* **2019**, 7. <https://doi.org/10.1186/s40635-019-0274-x>.
- [34] I. F. Ghalayini, *Int. J. Impotence Res.* **2004**, 16, 459.
- [35] E. J. Brisbois, H. Handa, T. C. Major, R. H. Bartlett, M. E. Meyerhoff, *Biomaterials* **2013**, 34, 6957.
- [36] M. F. Ebbesen, D. H. Schaffert, M. L. Crowley, D. Oupický, K. A. Howard, *J. Polym. Sci., Part A: Polym. Chem.* **2013**, 51, 5091.
- [37] J. Kopeček, H. Bažilová, *Eur. Polym. J.* **1973**, 9, 7.
- [38] T. Gresham, J. Jansen, F. Shaver, R. Bankert, F. Fiedorek, *J. Am. Chem. Soc.* **1951**, 73, 3168.
- [39] S. - P. Tao, J. Zheng, Y. Sun, *J. Chromatogr. A* **2015**, 1389, 104.
- [40] D. Tanini, A. Degl'Innocenti, A. Capperucci, *Eur. J. Org. Chem.* **2015**, 2015, 357.
- [41] M. Klapper, S. Nenov, R. Haschick, K. Mueller, K. Muellen, *Acc. Chem. Res.* **2008**, 41, 1190.
- [42] V. Jaitely, T. Sakthivel, G. Magee, A. Florence, *J. Drug Delivery Sci. Technol.* **2004**, 14, 113.
- [43] J. Bevington, T. Huckerby, B. Hunt, A. Jenkins, *J. Macromol. Sci., Part A* **2001**, 38, 627.
- [44] M. Johansson, A. Hult, *J. Polym. Sci., Part A: Polym. Chem.* **1991**, 29, 9.
- [45] Q. Yu, M. Zhang, X. Li, R. Bai, *Front. Chem. China* **2007**, 2, 414.
- [46] V. Zubov, M. V. Kumar, M. Masterova, V. Kabanov, *J. Macromol. Sci., Chem.* **1979**, 13, 111.
- [47] A. Musyanovych, V. Mailänder, K. Landfester, *Biomacromolecules* **2005**, 6, 1824.
- [48] D. Wei, M. Han, L. Yu, *Sci. Rep.* **2017**, 7, 6376.
- [49] A. Hosseinnejad, N. Ludwig, A.-K. Wienkamp, R. Rimal, C. Bleilevens, R. Rossaint, J. Rossaint, S. Singh, *Biomater. Sci.* **2022**, 10, 85.
- [50] E. van Andel, S. C. Lange, S. P. Pujari, E. J. Tijhaar, M. M. Smulders, H. F. Savelkoul, H. Zuilhof, *Langmuir* **2018**, 35, 1181.
- [51] H. Yuan, B. Yu, L.-H. Fan, M. Wang, Y. Zhu, X. Ding, F.-J. Xu, *Polym. Chem.* **2016**, 7, 5709.
- [52] E. J. Brisbois, *Novel Nitric Oxide (NO)-Releasing Polymers and Their Biomedical Applications*, **2014**.
- [53] A. Laschewsky, *Polymers* **2014**, 6, 1544.
- [54] A. Sinclair, M. B. O'Kelly, T. Bai, H. C. Hung, P. Jain, S. Jiang, *Adv. Mater.* **2018**, 30, 1803087.
- [55] N. Hogg, R. J. Singh, B. Kalyanaraman, *FEBS Lett.* **1996**, 382, 223.
- [56] D. Steinmann, T. Nauser, W. H. Koppenol, *J. Org. Chem.* **2010**, 75, 6696.
- [57] B. Alzua, M. Smith, Y. Chen, *Front. Biomed. Devices, Am. Soc. Mech. Eng.* **2020**, DMD2020, V001T01A010.
- [58] Q. Lu, R. A. Malinauskas, *Artif. Organs* **2011**, 35, E65 .
- [59] D. R. Phillips, I. F. Charo, L. V. Parise, L. A. Fitzgerald, **1988**, 71, 831.
- [60] D. Varga-Szabo, I. Pleines, B. Nieswandt, *Arterioscler., Thromb., Vasc. Biol.* **2008**, 28, 403.
- [61] R. L. Lundblad, G. C. White, *Platelets* **2005**, 16, 373.
- [62] A. Friebe, P. Sandner, A. Schmidtko, *Naunyn-Schmiedeberg's Arch. Pharmacol.* **2020**, 393, 287.
- [63] M. Park, P. Sandner, T. Krieg, *Basic Res. Cardiol.* **2018**, 113, 24.
- [64] J. K. T. Wentworth, G. Pula, A. W. Poole, *Biochem. J.* **2005**, 393, 555.
- [65] M. Hammes, *Biomed Res. Int.* **2015**, 2015, 171674.
- [66] P. M. Benz, H. Laban, J. Zink, L. Günther, U. Walter, S. Gambaryan, K. Dib, *Cell Commun. Signaling* **2016**, 14, 21.